

# Redox-Detecting Deep Learning for Mechanism Discernment in Cyclic Voltammograms of Multiple Redox Events

Benjamin B. Hoar,<sup>†</sup> Weitong Zhang,<sup>†</sup> Yuanzhou Chen,<sup>†</sup> Jingwen Sun, Hongyuan Sheng, Yucheng Zhang, Yisi Chen, Jenny Y. Yang, Cyrille Costentin,<sup>\*</sup> Quanquan Gu,<sup>\*</sup> and Chong Liu<sup>\*</sup>



Cite This: *ACS Electrochem.* 2025, 1, 52–62



Read Online

ACCESS |



Metrics & More



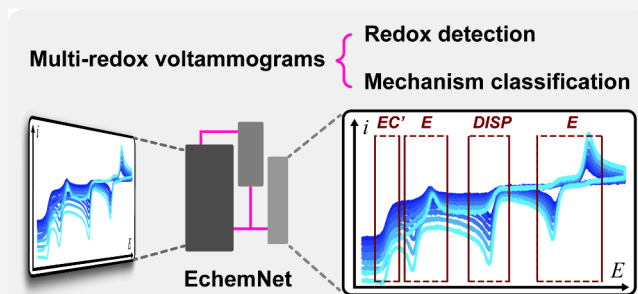
Article Recommendations



Supporting Information

**ABSTRACT:** In electrochemical analysis, mechanism assignment is fundamental to understanding the chemistry of a system. The detection and classification of electrochemical mechanisms in cyclic voltammetry set the foundation for subsequent quantitative evaluation and practical application, but are often based on relatively subjective visual analyses. Deep-learning (DL) techniques provide an alternative, automated means that can support experimentalists in mechanism assignment. Herein, we present a custom DL architecture dubbed as EchemNet, capable of assigning both voltage windows and mechanism classes to electrochemical events within cyclic voltammograms of multiple redox events. The developed technique detects over 96% of all electrochemical events in simulated test data and shows a classification accuracy of up to 97.2% on redox events with 8 known mechanisms. This newly developed DL model, the first of its kind, proves the feasibility of redox-event detection and electrochemical mechanism classification with minimal *a priori* knowledge. The DL model will augment human researchers' productivity and constitute a critical component in a general-purpose autonomous electrochemistry laboratory.

**KEYWORDS:** cyclic voltammetry, deep-learning, mechanistic assignment, autonomous laboratory



## INTRODUCTION

Cyclic voltammetry is one of the most popular analytical electrochemical techniques.<sup>1–4</sup> In fact, there is no need to look beyond the cover of many electrochemistry textbooks to see the famous “duck-shaped” plots of cyclic voltammograms.<sup>2–5</sup> The relationship between current density ( $i$ ) and applied potential ( $E$ ) as a function of multiple,  $n$ -numbered scan rates ( $\nu$ ), represented as  $\{i, i(E)\}_\nu$ , is necessary for an identification of reaction mechanisms with  $z$ -numbered redox events, in which each includes the combinations of electrochemical ( $E_{\text{step}}$ ) and possibly chemical ( $C_{\text{step}}$ ) reaction steps.<sup>2,3,6</sup> The mechanistic identification starts with visual inspections that not only descriptively inquire the voltammogram's shape but also quantitatively extract valuable mechanistic information including but not limited to the redox peak potential/current, half-wave width and/or plateau potential/current. Those quantitative visual inspection is a prerequisite to either formulating the partial differential equations (PDEs) and boundary/initial conditions for the downstream numerical simulations that extract quantitative thermodynamic and kinetic information,<sup>7</sup> or consulting literature results that were determined by the solution of those PDEs. Such hypothesized mechanism obtained from finite electrochemical data is also instructive towards the design of other non-electrochemical experiments, which collectively constitute a comprehensive mechanistic study that integrates all channels of experimental results.

Despite voltammetry's foundational place in the pantheon of electroanalytical tools, there is no consistent heuristic of visual inspection for voltammograms' use in mechanism assignment—perhaps the most common use of cyclic voltammetry.<sup>8</sup> Manual visual inspection of the scan rate's influence on voltammetric responses under different chemical concentrations remains the primary means of mechanism assignment. Reliance on manual inspection precludes any application in high-throughput systems, limits its utility for both experts and non-experts, and renders analysis intractable when cyclic voltammograms increase in complexity and noise.<sup>8–10</sup>

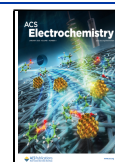
Recent advances in machine learning and artificial intelligence offer a new perspective on voltammogram inspection and mechanism assignment.<sup>8–10</sup> Machine-learning techniques have been applied to mechanistic classification of single-redox voltammograms,<sup>11–13</sup> and numerical fitting of voltammogram data under a pre-determined mechanistic assignment.<sup>14–16</sup> It is proposed that machine learning's expertise in pattern recognition and feature extraction<sup>17</sup> is

**Received:** June 26, 2024

**Revised:** August 30, 2024

**Accepted:** September 12, 2024

**Published:** October 3, 2024



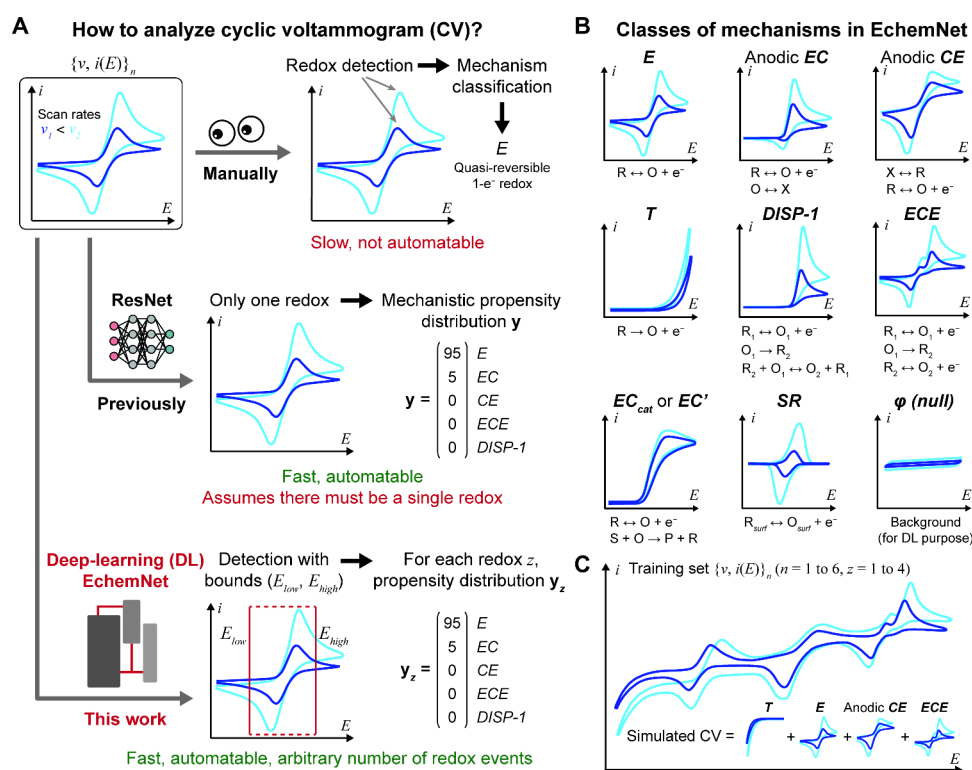


**Figure 1.** A, the comparison of different approaches to the analysis of cyclic voltammograms (CVs), including the deep-learning (DL) architecture based on Faster R-CNN (Regional Convolutional Neural Network) dubbed as EchemNet. B, the classes of electrochemical mechanisms included in EchemNet. C, exemplary illustration of simulated CVs of multiple redox events (multi-redox CVs) used as training set in this study. Each data point in the training set contains a set of multi-redox CVs with  $n$ -numbered scan rates and  $z$ -numbered redox events ( $\{v, i(E)\}_n$ ,  $n = 1$  to 6;  $z = 1$  to 4). The color of the voltammogram traces illustrates the scan rate  $v$ : the darker the color, the larger the value of  $v$ . ResNet, Residual neural network.

complementary if not substitutive to manual inspection of electrochemical data.<sup>11,12,18</sup> For example, our recent work reported a deep-learning (DL) model based on the architecture of ResNet (Residual Neural Network)<sup>19</sup> that automatically analyzes cyclic voltammograms (Fig. 1A), assuming the presence of only one redox event, and designates the probable mechanism among five of the most common ones in homogeneous molecular electrochemistry.<sup>12</sup> The ResNet model yields a probability distribution for five mechanisms, represented as a vector  $y = \{y_i\}$  ( $i = 1$  to 5) in which  $y_i$  refers to the mechanistic propensity of the  $i$ -th mechanism. Such a probability-driven analysis provides a more satisfying accommodation given the finite amount of available electrochemical data and the finite measurement resolutions of instrumentations. A DL-based analysis opens the opportunities of simultaneous data analysis for multiple electrochemical techniques, a feat untenable by humans owing to the data's nature of high dimensionality.<sup>8</sup>

The recent development of high-throughput electrochemistry calls for automated electrochemical analysis, potentially DL-based ones, with high data throughput. One new direction of electrochemical research is the development of high-throughput electrochemistry platforms for applications in battery, catalysis, and electrosynthesis.<sup>20–23</sup> The large data throughput of automated testing requires an equivalently high-throughput method of data analysis. Moreover, with the exciting development of hardware, the development of online data analysis, the prerequisite for on-line decision making hence a higher level of autonomy, is in greater demand. Indeed, our recent work demonstrates that integrating automated experimentation with ResNet-based voltammogram

analysis leads to autonomous research for homogeneous electrochemistry.<sup>20</sup> In parallel to the development of experimentation platform, it is equally important to develop a general purpose DL-based analysis for electrochemical data.

However, to date, the developed machine-learning models all require one piece of important *a priori* information, namely that the number of redox events  $z$  is presumably known ( $z = 1$  in previous reports<sup>11–13</sup>), which renders the DL models not entirely on par with manual inspection. In a typical manual inspection of voltammograms without any *a priori* information, human researchers first identify and locate any redox events in the voltammogram, *i.e.* a task of object detection, then determine the mechanism type for each redox event, *i.e.* a task of classification, before potentially establishing any correlation among redox events in search of causality. While reported algorithms are capable of mechanistic classification for single-redox events in voltammograms,<sup>11–13</sup> a DL algorithm, tasked with both object detection and classification, remains to be developed for automated analysis of cyclic voltammetry. As DL architecture such as Faster R-CNN (Regional Convolutional Neural Network)<sup>24</sup> has been widely used for the recognition and classification of two-dimensional images in a wide range of applications, we envision using Faster R-CNN architecture to develop a voltammogram-reading DL model with the functionalities of both redox-event detection and mechanism classification.

Here we report a custom-designed DL architecture based on Faster R-CNN, the first of its kind and dubbed as EchemNet, capable of both redox-event detection and mechanism classification for cyclic voltammograms of multiple redox events (multi-redox CVs) with minimal *a priori* information

(Fig. 1A). As voltammetry data  $\{v, i(E)\}_n$  are intrinsically sets of one-dimensional (1D) vectors instead of two-dimensional images, a custom-designed model of 1D Faster R-CNN architecture is developed to locate the potential window for up to 4 redox events ( $z \leq 4$ ) and designate the probable mechanism in a probabilistic manner (Fig. 1A). The EchemNet is trained by simulated multi-redox CVs of up to 6 scan rates and up to 4 independent redox events ( $\{v, i(E)\}_n$ ,  $n = 1$  to 6;  $z = 1$  to 4), categorized in 8 different reaction mechanisms spanning homogeneous, heterogeneous, and surface electrochemistry (Fig. 1B). The DL model exhibits an overall  $F_1$  score, a statistical combined measure of binary classification in accuracy and sensitivity,<sup>25</sup> of up to 0.937 towards redox-event detection and mechanism classification among simulated voltammograms, while preliminary testing with experimental data are satisfactory as well. Our work showcases the feasibility of a DL algorithm for voltammogram analysis without the need for any *a priori* knowledge, hence the genesis of a general-purpose autonomous platform of electrochemical research that augments the productivity of human researchers.

## RESULTS AND DISCUSSION

**A Training Set of Simulated Voltammograms of Multiple Redox Events (Multi-redox CVs).** The dataset that yields EchemNet includes simulated multi-redox CVs, conducted via finite-element methods using COMSOL Multiphysics v5.5 (Supplementary Note 1). What we sought is to establish a dataset of simulated voltammograms that sample the majority of if not the whole numerical parameter space for each mechanism as defined in textbooks<sup>2,3</sup> (Supplementary Note 2). Each data point in the dataset includes voltammograms of up to 6 scan rates and up to 4 redox events ( $\{v, i(E)\}_n$ ,  $n = 1$  to 6;  $z = 1$  to 4).

Eight common mechanisms in electrochemistry (Fig. 1B) have been included following the textbook definitions (Supplementary Note 3):<sup>2,3</sup> (1) the single-electron quasi-reversible homogeneous electron transfer ( $E$ ); (2) a single-electron quasi-reversible homogeneous oxidative electron transfer followed by a chemical reaction of the oxidant in the solution (anodic  $EC$ ); (3) a single-electron quasi-reversible oxidative electron transfer preceded by a chemical reaction of the reductant in the solution (anodic  $CE$ ); (4) the single-electron heterogeneous electron transfer following the Tafel kinetics ( $T$ ), when the heterogeneous concentration-dependent Butler-Volmer kinetic is irreversible (no back reaction) at relatively large overpotentials; (5) the two-electron homogeneous electron transfer, in which a single-electron transfer is followed by an irreversible, rate-determining chemical step and a disproportionation step ( $DISP-1$ ); (6) a similar two-electron homogeneous electron transfer, in which a single-electron transfer is followed by an irreversible chemical step and a thermodynamically less demanding single-electron transfer ( $ECE$ ); (7) the homogeneous electrocatalysis, in which a single-electron transfer is followed by a chemical step that regenerates the redox-active catalyst ( $EC_{cat}$  or  $EC'$ ); (8) the interfacial single-electron transfer when the redox species follows the Butler-Volmer kinetics and is bound on the electrode surface ( $SR$ ). Here we emphasize that the categorization of  $EC$  and  $CE$  mechanisms are defined as the anodic scan of voltammogram is considered the “forward” direction, because an anodic/cathodic  $EC$  mechanism is

mathematically equivalent to a cathodic/anodic  $CE$  one, respectively, following the textbook definitions.<sup>2,3</sup>

One fundamental assumption that we impose when establishing the dataset of simulated voltammograms is that the redox reactions are independent to each other. This assumption pertains to the scenarios when multiple redox species of relatively dilute concentrations coexist in the electrolyte solution, and the reactants/products of redox reactions do not interfere with each other. Despite the foreseeable practical relevance in electrochemical analysis, typically conducted in diluted solutions, this assumption does not include the scenarios when a single chemical species undergo multiple redox events or multiple redox species are interconnected via chemical reactions ( $C$  steps). However, we contend that our assumption should suffice to demonstrate the feasibility and proof-of-concept of analyzing voltammograms with DL models. Technically, it is much more challenging to implement finite-element simulations for arbitrary combinations of multiple redox systems with sufficiently high simulation throughput. More discussion regarding this limitation can be found in Supplementary Note 2.

A multi-step process is developed to establish the dataset of simulated multi-redox CVs. First, the parameter space of each mechanism, for example the value ranges for scan rate ( $v$ ), exchange current density ( $i_0$ ), equilibrium constant ( $K$ ), forward kinetic rate constant ( $k_f$ ) in the  $EC$  mechanism, as well as redox species' diffusion coefficient ( $D$ ) and initial concentration ( $C_{R,i}$ ), are carefully defined following textbooks and prior literature<sup>2,3</sup> (Table S1, Supplementary Note 3). Second, we randomly sampled about 3,000 parameter combinations following the constraints defined in Table S1, for each mechanism type with up to 6 different scan rates ( $n = 1$  to 6). Third, from the available 8 mechanisms and about 24,000 ( $= 8 \times 3000$ ) parameter combinations, we randomly selected no more than 4 parameter combinations ( $z = 1$  to 4) and deployed finite-element simulations to yield simulated multi-redox CVs, with randomized redox sequences, voltage spacings among every redox event, and relative concentrations of redox species that dictate the current densities  $i$  among different redox features (Fig. 1C).

About 80,000 data points of simulated multi-redox 6-scan CVs ( $\{v, i(E)\}_n$ ,  $n = 6$ ;  $z = 1$  to 4), about 480,000 ( $= 6 \times 80,000$ ) voltammograms in total, were generated. The number of generated voltammograms is much smaller than the theoretical value of about  $10^{17}$  different combinations of parameters for simulated multi-redox CVs based on the above protocol (mathematically calculated based on the permutation expression  $P_4^{24,000} = 24,000!/(24,000-4)!$ ). As shown below, such a relatively small amount of data is sufficient for the DL model's establishment, among which 90% of these data points are the training data and the rest 10% are the test data (Supplementary Note 1).

Some additional assumptions are made when establishing the data set of simulated multi-redox CVs. As we aim to demonstrate the DL's feasibility in analyzing multi-redox CVs first, the voltammograms in the proof-of-concept training set assume that each redox event is independent to each other (Supplementary Note 2). We also ensure that the training set includes well-separated redox peaks, and the current densities of redox peaks are on the same order of magnitudes among all redox events (Supplementary Note 4).

**Definition of the Model's Input, Outputs, and Ground Truth.** The establishment of DL model requires

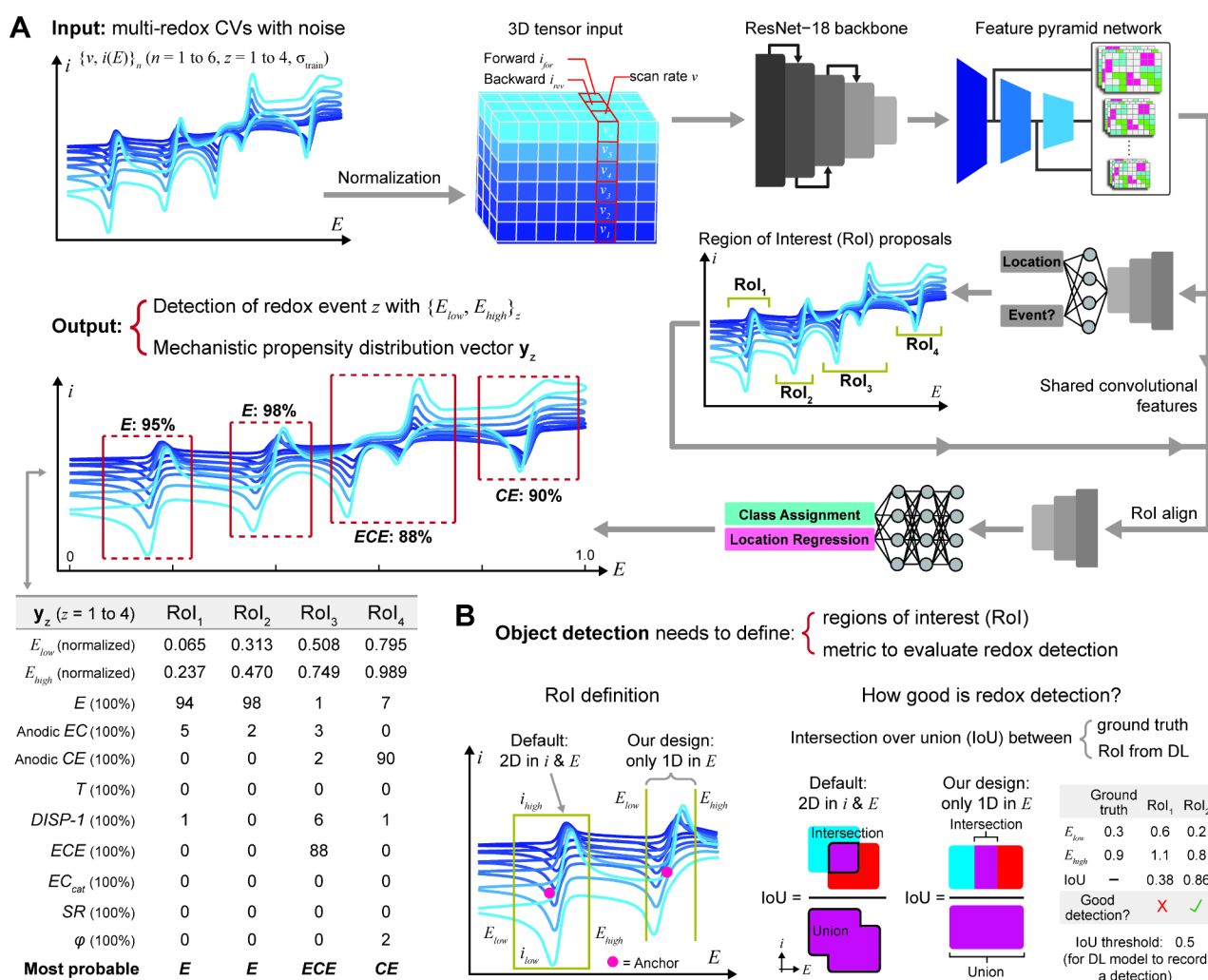


**Figure 2.** A, The input, outputs, and general architecture of the deep-learning (DL) model, “EchemNet”, tailored to the analysis of multi-redox CVs. B, Highlights in the custom-designed model that includes one-dimensional (1D) regions of interest (RoIs) and the calculation of Intersection over Union (IoU), in comparison to the default two-dimensional (2D) one used in image recognition. The use of 1D RoI, a certain voltage range in the voltammogram generated by the DL model for a proposed detection of redox events, ensures that object detection will not be inadvertently affected by the magnitude of current density  $i$  and will not lose sensitivity towards small redox features. In our 1D redox-detection model, the IoU is calculated as the ratio of the voltage-range overlap between the RoI and ground truth of  $E_{\text{low}}$  and  $E_{\text{high}}$  (“Intersection”) to the combined voltage range between the RoI and ground truth (“Union”).

explicit definitions about the model’s input, outputs, and the corresponding “ground truths” for the outputs. Below we discuss these items based on the dataset of 480,000-large simulated multi-redox CVs established in the previous section.

The DL model’s input is the multi-redox 6-scan CVs ( $\{v, i(E)\}_n$ ,  $n = 1$  to 6;  $z = 1$  to 4). More specifically, a data structure of three-dimensional tensor with a size of  $(6 \times 3 \times 1000)$  was deployed following our previous work.<sup>12</sup> Each input tensor records the normalized voltages  $E_{\text{normalized}}$ , normalized current densities  $i_{\text{normalized}}$  of both forward and backward scan, as well as the absolute values of scan rate  $v_n$ , for one set of multi-redox 6-scan CVs (Supplementary Note 5).

To increase the robustness of the developed DL model (see below), a certain extent of Gaussian noise was applied to the normalized current density  $i_{\text{normalized}}$  (Supplementary Note 5) following the same protocol as our previous work.<sup>12</sup> When adding the Gaussian noise, each data point of normalized current  $i_{\text{normalized}}$  is added with a random value of noise, whose probability follows a normal distribution with a dimensionless standard deviation  $\sigma$ . We denote  $\sigma_{\text{train}}$  when this noise is added

to the simulated voltammograms during the training process of DL model, while  $\sigma_{\text{test}}$  is denoted when the noise is added during to the simulated voltammograms during the testing for the trained DL model.  $\sigma_{\text{train}} = \sigma_{\text{test}} = 0.01$  unless otherwise noted

Mathematically, a Gaussian noise can be Fourier transformed in the frequency domain with equal weights for all possible sequences. Hence the added noises our simulated voltammograms contain frequency components across all frequency values up to the frequency of data sampling. Thanks to its stochastic nature, Gaussian noise is a good representation for thermal fluctuations during experimental electric measurement.<sup>26</sup> However, we acknowledge that it may not represent noises from other origins, for example from the intrinsic properties of the operational amplifiers (op-amps) and high/low-pass filters.

One type of outputs from the DL model is the voltage window, presented as the cathodic and anodic voltage bounds, for each redox event in voltammograms. As there are at most four redox events in the simulated voltammogram training set,



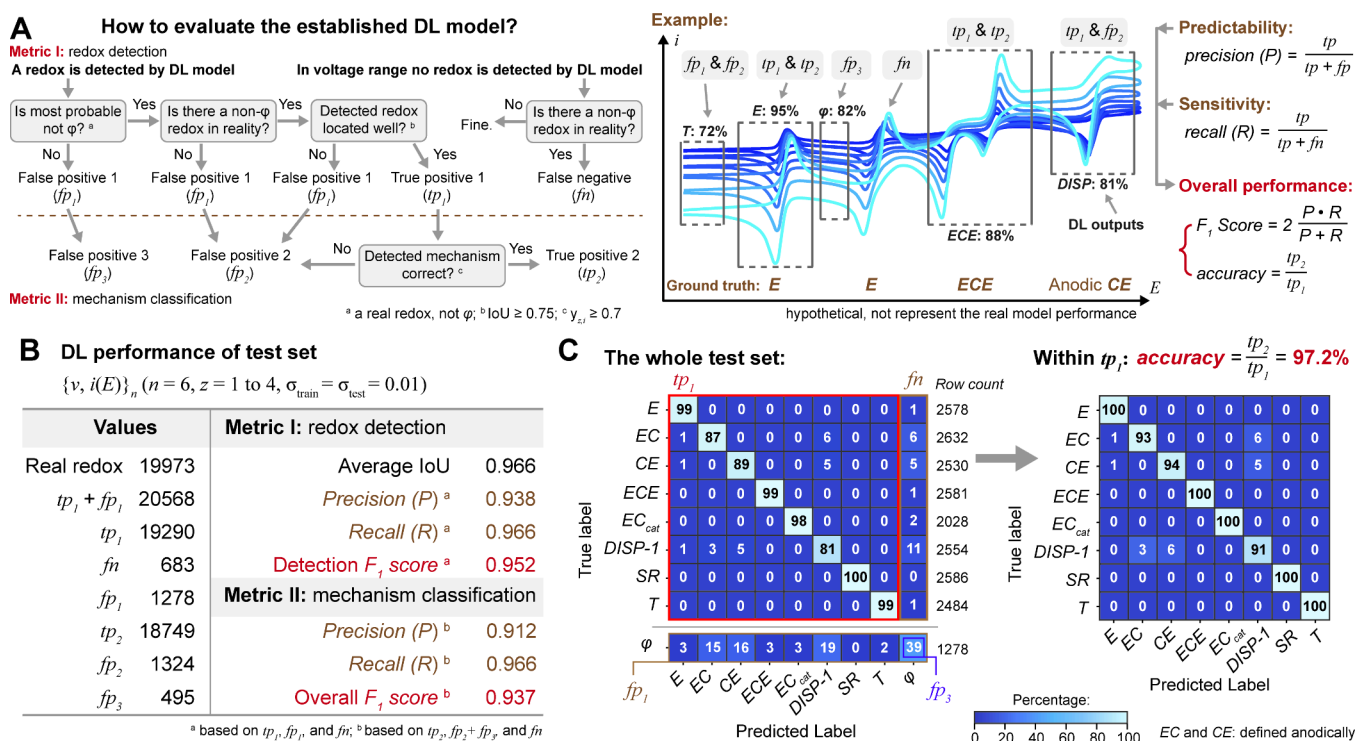


**Figure 3.** A, Explanations and the logical flow chart of the true positives, false positives, and false negatives in the established EchemNet model for both redox-event detection and mechanism classification, along with the definitions of metrics for performance evaluation. B, The assay of test-set voltammograms and the DL model's performance. The test set is roughly 10% of the whole dataset of simulated voltammograms (Supplementary Note 1). C, Confusion matrix, a commonly deployed performance evaluation tool that represents the accuracy of a classification model, from the test-set assay for the whole test set (left) and within the cases of true positive 1 ( $tp_1$ ) after redox-event detection (right). Row count, the number of encounters when the corresponding mechanism on the row of "True label" were analyzed in the test set.

one to four pairs of the cathodic and anodic voltage bounds, denoted as  $E_{\text{low}}$  and  $E_{\text{high}}$ , respectively, are expected to be determined by the DL model from the input tensor of 6-scan voltammograms. The  $E_{\text{low}}$  and  $E_{\text{high}}$  outputs are normalized voltage values, as the DL model receives normalized voltages  $E_{\text{normalized}}$  as inputs. The use of  $E_{\text{low}}$  and  $E_{\text{high}}$  to represent the voltage window without the information on current density  $i$  is consistent with our design of one-dimensional (1D) object-detection model (see below).

The other type of outputs from the DL model is the propensity distribution of probable mechanisms for each detected redox event. Here we define the one-dimensional vector  $y_z = \{y_{z,i}\}$  ( $i = 1$  to 9) as the mechanistic propensity distribution for the  $z$ -th detected redox event. In this 9-component vector  $y_z$ ,  $y_{z,i}$  ( $i = 1$  to 8) denotes the predicted probability for the aforementioned 8 mechanisms in their discussed order. A 9th component  $y_{z,9}$  is added to denote the residual predicted probability of the background double-layer charging, noted as  $\varphi$  class, whose voltammetric feature is also displayed in Fig. 1B. Not only will the inclusion of  $\varphi$  class offers a semi-quantitative evaluation of the redox feature's prominence amid the background of double-layer charging, the inclusion of  $\varphi$  class is indeed consistent with the architecture of DL algorithm in which there is always a "null" category whose probability indicates the extent of inability in classification.<sup>19,24</sup>

The "ground truth" of the DL-based analysis is also established. In statistics and machine learning, the term "ground truth" is defined as the knowledge of the truth concerning a specific question. Specific in our works, the ground truth of specific multi-redox 6-scan CVs corresponds to

the known values of redox features' voltage positions and their corresponding underlying mechanism. The ground truth of redox features' voltage positions are represented by the known values of  $E_{\text{low}}$  and  $E_{\text{high}}$ , which were calculated following a uniform protocol for each redox event in the simulated voltammogram (Supplementary Note 4). The ground truth of redox's underlying mechanism is presented by designating the corresponding  $y_{z,i} = 1$  for the mechanism under which the voltammograms were simulated, and  $y_{z,i} = 0$  for all the other ones. The voltammogram data  $\{v, i(E)\}_n$  and the corresponding ground truth  $E_{\text{low}}$  and  $E_{\text{high}}$  were normalized before being deployed for the model's training, validation, and testing (Supplementary Note 5).

**Design of Deep-Learning (DL) Architecture.** A custom-designed Faster R-CNN architecture was needed to establish the EchemNet model. The presence of multiple electrochemical events/mechanisms within a single cyclic voltammogram precludes the use of image classification algorithms such as ResNet<sup>19</sup> alone. Alternatively, convolutional layer-based algorithms, specifically object detection algorithms, can be considered as a mature technology for the elucidation of electrochemical mechanisms contributing to a convoluted  $\{v, i(E)\}_n$  output. One such architecture, Faster R-CNN,<sup>20</sup> is selected. In such a DL architecture, an online region proposal network (RPN) is trained end-to-end to perform the tasks of both redox detection and mechanistic classification (Fig. 2A), with the deployment of feature pyramid networks<sup>27</sup> that promote multi-scale detections.

However, the intrinsic feature of voltammograms, and more broadly electrochemical data in general, calls for a 1D adaptation of the DL architecture. Although typical algorithms

of Faster R-CNN are developed for the analysis of two-dimensional (2D) images,<sup>24</sup> object detection in voltammograms is intrinsically a one-dimensional (1D) task, because from a chemistry perspective the location of every redox event should only be  $E$ -dependent in voltammograms. A deployment of 2D object detection in voltammograms will explicitly introduce the magnitude of current density  $i$  as a criterion of redox-event detection, inadvertently position a bias towards large redox events and significantly decrease the detection sensitivity towards small ones.

Hence, we employed the tools in Faster R-CNN with 1D custom implementation. A custom-designed 1D RPN generates a region of interest (RoI), defined as a certain voltage range ( $E_{\text{low}}$  and  $E_{\text{high}}$ ) proposed by the DL model, for possible detection of a redox event (Fig. 2A). During the training and validation of DL model, the RoIs generated from RPN are then compared with the ground truths of  $E_{\text{low}}$  and  $E_{\text{high}}$  defined in the earlier section, to evaluate the model's accuracy of redox detection. In typical 2D image recognition, the algorithm evaluates the performance of object detection with the term named as Intersection over Union (IoU), which is calculated as the ratio of the overlap area ("Intersection") to the combined area ("Union") between an algorithm-detected object and the corresponding ground truth in a 2D image (hence  $\text{IoU} \in [0,1]$ ) (Fig. 2B). In accordance with the 1D adaptation of RPN and RoI, to assess the quality of object detection, 1D IoU was calculated as the ratio of the overlap voltage range to the combined one between algorithm-yielded voltage window ( $E_{\text{low}}$  and  $E_{\text{high}}$ ) and the corresponding ground truth ( $\text{IoU} \in [0,1]$  as well) (Fig. 2B). As shown later, a value of  $\text{IoU} \geq 0.75$  is considered a satisfactory detection of the redox feature by the DL algorithm. The deployment of 1D RoI and IoU provides high fidelity between the bounds of known and predicted redox events in voltammograms, leading to an algorithm with a highly effective means of mechanism enumeration from complex voltammogram data (Fig. 2A and S1, Supplementary Note 5).

The algorithm also deploys ResNet, as reported in our previous work,<sup>12</sup> for the classification in each RoI among the aforementioned 8 mechanisms and the null class ( $\varphi$ ) that indicates the voltammogram background without any designated redox events (Fig. 1A). It takes about 12 h to train the DL model for about 100,000 epochs. As exemplified in Fig. 2A, the developed EchemNet after satisfactory training (Fig. S2) is designed to discern multi-redox CVs and enumerate the voltage window of the  $z$ -th detected redox event ( $\text{RoI}_z$ ) represented as normalized voltage values ( $E_{\text{low}}$  and  $E_{\text{high}}$ ), the corresponding mechanistic propensity distribution  $\mathbf{y}_z = \{y_{z,i}\}$  ( $i = 1$  to 9) towards the trained 8 redox mechanisms plus  $\varphi$  class, and the assignment of the most probable mechanism.

**Performance Evaluation.** There are two separate yet related metrics for the evaluation of a DL model for both object detection and classification: Metric I, the effectiveness of the RPN to detect events independent of their mechanism, *i.e.* performance in redox detection alone; Metric II, the overall inference performance which is the combination of redox detection (matching of predicted voltage windows with the ground truth) and classification (matching of the predicted most probable mechanism with the ground truth) of the RoIs provided by the RPN (Fig. S1).

In the evaluation of object detection alone (Metric I, Fig. 3A), 3 different outcomes are possible through the course of

region proposal and object detection: RoIs represented as  $E_{\text{low}}$  and  $E_{\text{high}}$  predicted by the RPN could ultimately align with ground truth of redox bounds (object detection true positive,  $tp_1$ ; when  $\text{IoU} \geq 0.75$  between the algorithm-yielded proposed redox voltage window and the corresponding ground truth) or not (object detection false positive,  $fp_1$ ), and regions where known true redox bounds were not detected were assigned as false negatives ( $fn$ ).

In the evaluation of overall inference performance (Metric II, Fig. 3A), a true positive ( $tp_2$ ) is logged when the ground truth mechanism  $i$  for the  $z$ -th detected redox is confidently denoted as the most probable mechanistic propensity in  $\mathbf{y}_z$  vector ( $y_{z,i} \geq 0.7$ ) with good overlap with the redox's voltage bounds ( $\text{IoU} \geq 0.75$ ); while the false positives are further categorized based on whether the model-yielded RoIs detect a real redox event ( $fp_2$ ) or merely detect  $\varphi$  background ( $fp_3$ ) (Fig. 2A). There is no delineation between the false negatives ( $fn$ ) between object detection (Metric I) and overall inference (Metric II), hence the  $fn$  sub-population remains the same to the evaluation of object detection and overall inference metrics.

The developed DL model was evaluated for its performance, in a protocol similar to our previous report,<sup>12</sup> after being trained by simulated multi-redox CVs ( $\{v, i(E)\}_m$ ,  $n = 6$ ;  $z = 1$  to 4;  $\sigma_{\text{train}} = 0.01$ ). The test set for the DL model includes about 8,000 points of 6-scan voltammograms, 10% of the whole dataset that were not exposed to the developed DL model during the training process. The DL model exhibits an average IoU of 0.966 among the test set, where unity constituted a perfect overlap of predicted bounds with ground truth voltage windows (Fig. 3B). This is remarkable since within the DL algorithm a threshold value of IoU for a satisfactory redox detection is only 0.75.

Following the protocol of statistical analysis in image recognition and more generally binary classification,<sup>21</sup> the precision ( $P$ ) and recall ( $R$ ) of both metrics are calculated to evaluate the predictability and sensitivity, respectively, of the DL model (Fig. 3A). Here  $P$  is calculated as the percentage of true positives ( $tp$ ) among the sum of  $tp$  and false positives ( $fp$ ), which represents the accuracy of detecting correct redox features among all the detected ones;  $R$  is calculated the percentage of true positives ( $tp$ ) among the sum of  $tp$  and false negatives ( $fn$ ), which represents the sensitivity of not missing any detections of real redox features. Calculating the harmonic means of  $P$  and  $R$  in both metrics lead to the  $F_1$  scores, an overall measure of a model's performance whose calculation is shown in Fig. 3A.<sup>25</sup> A DL model of high  $F_1$  score is not only accurate in detecting redox features without much incorrect ones, but also sensitive enough to not miss any real redox features. As shown in Fig. 3B, the  $F_1$  scores in Metrics I and II reach 0.952 and 0.937, respectively, illustrating strong performance by the RPN (Metric I) and overall balanced performance with high values of both precision and recall (Metric II). Such a performance is satisfactory to say the least, based on the standard of image recognition,<sup>21</sup> within our aforementioned assumptions and our dataset of simulated voltammograms.

We also evaluated the class-by-class accuracies from the developed EchemNet model. As the developed ResNet classifies RoI into not only the 8 designated electrochemical mechanisms but also the null class ( $\varphi$ ), *i.e.* the background without any redox events, we first established a confusion matrix that includes 8 mechanisms and the  $\varphi$  events with  $tp_1$ ,

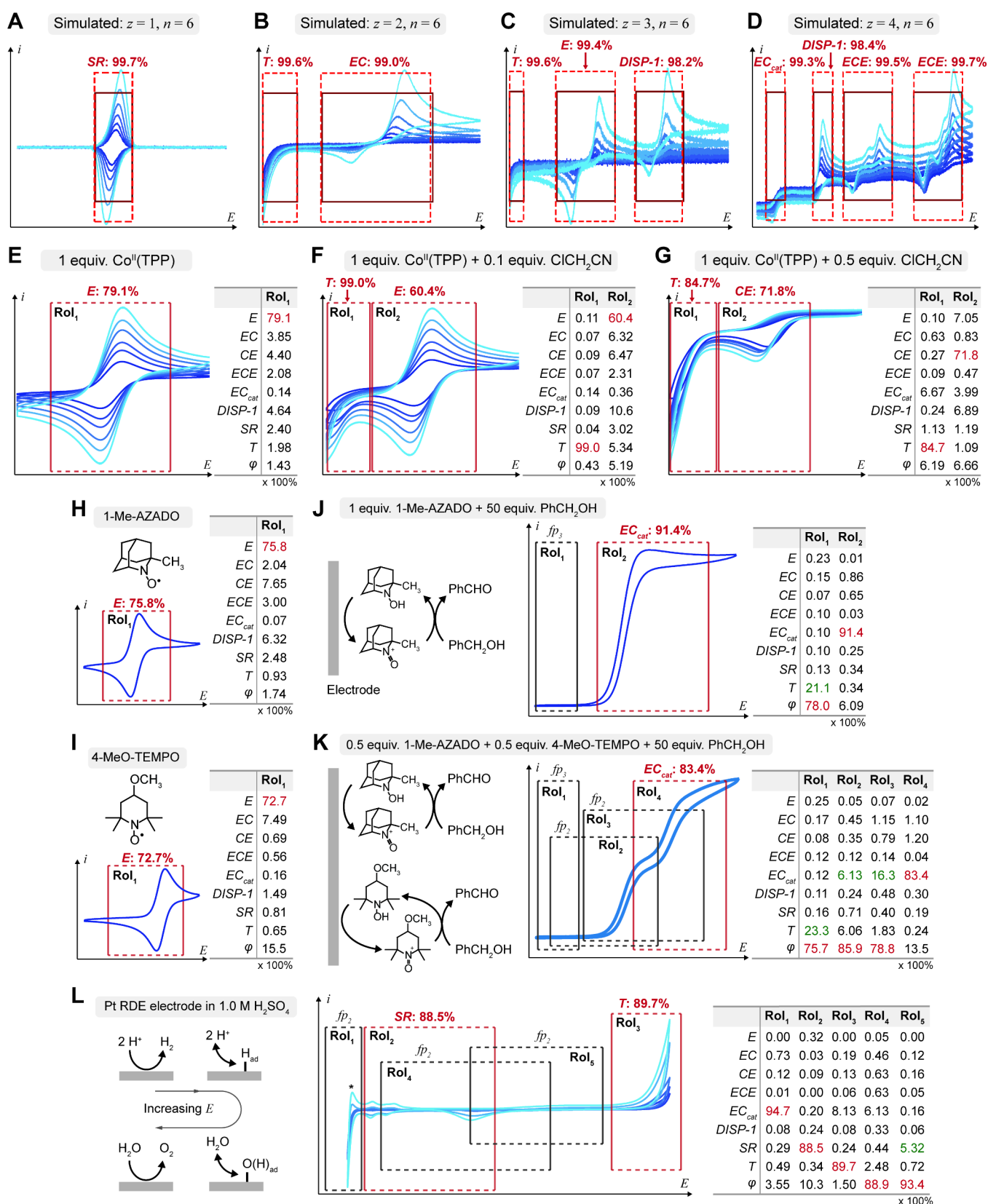


**Figure 4.** A to D, simulated voltammograms of 6 different scan rates ( $\nu = 6$ ) with 1, 2, 3, and 4 redox events ( $z = 1, 2, 3,$  and  $4$ ), respectively. The most probable mechanisms from the DL model, also the ground truths, are labelled with corresponding propensity values. The solid dark-red rectangles denote the ground truths of redox's voltage windows ( $E_{\text{low}}$  and  $E_{\text{high}}$  in Supplementary Note 4), and the dashed ones of bright-red color denotes the DL-generated Rols. E to G, experimental voltammograms of 1 mM cobalt(II) tetraphenylporphyrin ( $\text{Co}^{\text{II}}\text{TPP}$ ) alone (E), and with 0.1 mM and 0.5 mM chloroacetonitrile ( $\text{ClCH}_2\text{CN}$ ) (F and G, respectively). 0.1 M tetrabutylammonium hexafluorophosphate ( $\text{NBu}_4\text{PF}_6$ ) in dimethylformamide (DMF); Ar glove box; 3 mm glassy carbon disk working electrode;  $-1.5$  V to  $-0.9$  V vs.  $\text{Ag}/\text{Ag}^+$  (10 mM  $\text{AgNO}_3$  in acetonitrile) reference electrode; Pt wire counter electrode; 10, 20, 30, 50, 70, and 100 mV/s; 3<sup>rd</sup> cycle;  $iR$ -compensated; The formal potential for



Figure 4. continued

the  $\text{Co}^{\text{II/III}}$ /TPP redox was determined as  $-1.278$  V versus ferrocene/ferrocenium ( $\text{Fc}/\text{Fc}^+$ ). **H** to **K**, experimental voltammograms of 1 mM 1-methyl-2-azaadamantane-*N*-oxyl (1-Me-AZADO) alone (**H**), 1 mM 4-methoxy-2,2,6,6-tetramethylpiperidine-1-oxyl (4-MeO-TEMPO) alone (**I**), 1 mM 1-Me-AZADO with 50 mM benzyl alcohol ( $\text{PhCH}_2\text{OH}$ ) (**J**), and 0.5 mM 1-Me-AZADO and 0.5 mM 4-MeO-TEMPO with 50 mM  $\text{PhCH}_2\text{OH}$  (**K**). 0.15 M  $\text{NaHCO}_3/\text{Na}_2\text{CO}_3$  buffer (pH 9.14); Ambient conditions in  $\text{N}_2$ ; 3 mm glassy carbon disk working electrode; 0.05 to 0.85 V vs. Saturated Calomel Electrode (SCE); Pt wire counter electrode; 50 mV/s; 3<sup>rd</sup> cycle; *iR*-compensated. **L**, experimental voltammograms of Pt disk electrode in 1 M  $\text{H}_2\text{SO}_4$  under  $\text{N}_2$  atmosphere.  $-0.25$  V to 1.6 V vs. Ag/AgCl (3 M KCl) reference electrode; Pt wire counter electrode; 10, 20, 50, 100, 200, mV/s; 3<sup>rd</sup> cycle; *iR*-compensated. \*, the feature of  $\text{H}_2$  re-oxidation. The RoIs from EchemNet and the corresponding propensity distribution vectors  $y_z$  towards 8 mechanisms plus background ( $\varphi$ ) are all labelled in **E** to **L**. The voltammograms plotted in **E** to **L** have been normalized in both axes so that the exact  $E$  and  $i$  values are not displayed. More information about experimental methods is available in [Supplementary Note 6](#).

$f_n$ ,  $fp_1$ , and  $fp_3$  events highlighted (left in [Fig. 3C](#)). In machine learning, a confusion matrix is a commonly deployed performance evaluation tool that represents the accuracy of a classification model. Each row in the plots of [Fig. 3C](#) enlists the percentage of redox features, simulated based on a designated mechanism (“true label” in [Fig. 3C](#)), that are classified into a specific mechanism (“predicted label” in [Fig. 3C](#)). The number of encounters for each mechanism in the test set (“Row counts” in [Fig. 3C](#)) is relatively homogenous among all mechanisms, illustrating a fair and balanced test to the DL model. As shown in the left plot of [Fig. 3C](#), accurate mechanistic classification is achieved among mechanisms.

We further revised the “confusion matrix”, shown as the right plot of [Fig. 3C](#), to better reflect the accuracy of the DL model in practical applications. Practically, the DL’s functionality in the context of mechanism classification will not be affected by the presence of  $fp_1$  cases with  $\varphi$  prediction (hence  $fp_3$ ), contributing to 39% of total  $fp_1$  cases, when the DL algorithm unnecessarily yet correctly identifies a voltage window in the voltammogram that does not have any redox events and can be easily dropped in our model. Therefore, we plotted a revised confusion matrix among all  $tp_1$  cases, with a  $tp_2$  accuracy of 97.2%, presumably better reflecting the model’s utility in mechanistic analysis (right in [Fig. 3C](#)). Our results suggest that *DISP-1* mechanism is the most confused one, evident from non-negligible probabilities of mis-assigning a *DISP-1* mechanism as *EC/CE* one, or vice versa. Such phenomenon is similar to the one observed in our previous report of ResNet architecture for mechanism classification when only one redox event is known to exist.<sup>12</sup> The results reflect the similarity in voltammograms among *DISP-1* and *EC/CE* mechanisms, as depicted in the textbooks,<sup>2,3</sup> when the single-electron (*EC/CE*) and two-electron processes (*DISP-1*) are both under pure kinetic conditions.

While not detailed here, there are two more important metrics for the developed DL model: the robustness towards noises and the sensitivity of detecting small redox features. We analyzed those two metrics ([Fig. S3 and S4](#)) and provided our insights towards those two features can be found in [Supplementary Note 7](#). In short, we consider the developed model robust and sensitive for data taken under good experimental practices.

**Deployment Examples.** We first illustrate the utility of the developed EchemNet model via analyzing simulated voltammograms. [Fig. 4A](#) to [4D](#) display the simulated voltammograms ( $\{v, i(E)\}_n$ ,  $n = 6$ ,  $\sigma_{\text{rest}} = 0.01$ ) with the number of redox events  $z = 1, 2, 3$ , and 4, respectively, which was new to the trained DL model. The solid dark-red rectangles denote the redox events’ voltage windows ( $E_{\text{low}}$  and  $E_{\text{high}}$ ), derived based on our protocol and designated as the ground truth ([Supplementary Note 4](#)), while the dashed ones

of bright-red color denote the RoIs generated from EchemNet’s analysis. The close match between the designated ground truths and the analyzed RoIs suggest satisfactory performance of object detection with a IoU threshold value of 0.75 ( $tp_1$  in [Fig. 3A](#)). Moreover, each detected redox event is subject to mechanistic classification via the ResNet architecture. The most probable mechanism for each redox  $z$  ( $\text{RoI}_z$ ) is labelled on the voltammograms along with the corresponding propensity  $y_{z,i}$ , while the DL model outputs the whole  $y_z$  vector of mechanistic propensities. The high  $y_{z,i}$  values for the correctly predicted mechanisms illustrate the model’s high analytic fidelity. Statistically, our testing of about 8,000 points of simulated 6-scan voltammograms report the  $tp_2$  accuracies of 98.2%, 97.8%, 97.2%, and 96.6%, when  $z = 1, 2, 3$ , and 4, respectively. Such results indicate that despite slight decay the  $tp_2$  accuracy is relatively insensitive against the number of redox events ( $z$ ) and the developed DL model is robust against the increasing complexity in the voltammograms.

We deployed the EchemNet to analyze experimental data in exemplary chemical systems. Cobalt(II) tetraphenylporphyrin ( $\text{Co}^{\text{II}}$ /TPP) is known to undergo a quasi-reversible one-electron charge transfer ( $E$  mechanism) between formally  $\text{Co}(\text{II})$  and  $\text{Co}(\text{I})$  redox states ( $\sim -0.785$  V vs. Saturated Calomel Electrode, SCE<sup>24</sup>) in dimethylformamide (DMF) ([Supplementary Note 6](#)). From experimental voltammograms ( $n = 6$ ), such an  $E$  mechanism was correctly detected and classified by the DL model based on both RoI alignment and the corresponding  $y_z$  vector that includes mechanistic propensities of 8 mechanisms plus background ( $\varphi$ ) ([Fig. 4E](#)).

When chloroacetonitrile ( $\text{ClCH}_2\text{CN}$ ) was added to the solution of  $\text{Co}^{\text{II}}$ /TPP, the electrogenerated  $\text{Co}(\text{I})$  species nucleophilically attacked  $\text{ClCH}_2\text{CN}$  electrophile and yielded  $\text{Co}(\text{III})-\text{CH}_2\text{CN}$ , rendering the  $\text{Co}(\text{II})/\text{Co}(\text{I})$  redox irreversible (predicted by the model as *CE* mechanism due to its cathodic nature). At a more cathodic potential ( $< \sim -1.0$  V vs. SCE<sup>28</sup>), the yielded  $\text{Co}(\text{III})-\text{CH}_2\text{CN}$  species is reported to undergo multiple steps in a catalytic fashion, yielding voltammogram responses resembling either a  $T$  or  $EC_{\text{cat}}$  mechanism.<sup>28</sup> At a small equivalent of  $\text{ClCH}_2\text{CN}$  ([Fig. 4F](#)), the DL model correctly detects and classifies the catalytic process at more cathodic potentials ( $\text{RoI}_1$ ), while detecting the  $\text{Co}(\text{II})/\text{Co}(\text{I})$  redox and classifies it as an  $E$  mechanism ( $\text{RoI}_2$ ), albeit with a much lower propensity ( $y_E = 60.4\%$  in [Fig. 4F](#) against 79.1% in [Fig. 4E](#)), consistent with the increase of irreversibility owing to the reaction between  $\text{Co}(\text{I})$  and  $\text{ClCH}_2\text{CN}$ .<sup>24</sup> At a larger equivalent of  $\text{ClCH}_2\text{CN}$  ([Fig. 4G](#)), similar catalytic ( $\text{RoI}_1$ ) and  $\text{Co}(\text{II})/\text{Co}(\text{I})$  ( $\text{RoI}_2$ ) features are detected from the voltammograms, yet now the  $\text{Co}(\text{II})/\text{Co}(\text{I})$  redox is so irreversible that the most probable mechanism is assigned as *CE* (71.8%), indicative a greater extent of the reaction between  $\text{Co}(\text{I})$  and  $\text{ClCH}_2\text{CN}$ . The DL analysis of the



electrochemical data for  $\text{Co}^{\text{II}}\text{TPP}$  in the presence of  $\text{ClCH}_2\text{CN}$  is satisfactory.

We then challenged the DL model to analyze the redox and catalysis of nitroxyl derivatives in aqueous solutions,<sup>29,30</sup> but now with only a single voltammogram curve ( $n = 1$ ) instead of the default value of 6 (Supplementary Note 6). This is intended to test whether the DL model, while trained by  $\{v, i(E)\}_n$  ( $n = 6$ ), is applicable towards electrochemical datasets with a smaller number of scan rates. As implemented in our prior work,<sup>12</sup> we populated the 3D input tensor with 6 identical voltammograms and scan rates and fed the tensor into the DL model for analysis (Supplementary Note 5).

Quasi-reversible redox features of an  $E$  mechanism were successfully detected and classified by the DL model for 1-methyl-2-azaadamantane- $N$ -oxyl (1-Me-AZADO) (Fig. 4H) and 4-methoxy-2,2,6,6-tetramethylpiperidine-1-oxyl (4-MeO-TEMPO) (Fig. 4I). When benzyl alcohol ( $\text{PhCH}_2\text{OH}$ ) substrate is added to the solution of 1-Me-AZADO, two-electron electrocatalytic oxidation of  $\text{PhCH}_2\text{OH}$  via the  $EC_{\text{cat}}$  (or  $EC'$ ) mechanism emerges (Fig. 4J).<sup>3,29,30</sup> Such voltammetric response is correctly detected and identified ( $\text{RoI}_2$ ), yet a false positive ( $fp_3$ ) is also yielded with a  $y_\varphi = 78.0\%$  ( $\text{RoI}_1$ ).

When  $\text{PhCH}_2\text{OH}$  is added to a mixture of 1-Me-AZADO and 4-MeO-TEMPO, both 1-Me-AZADO and 4-MeO-TEMPO serve as  $EC_{\text{cat}}$  electrocatalysts in parallel, albeit at different catalytic onset potentials (Fig. 4K).<sup>29</sup> The resultant voltammogram display a two-step staircase shape, which was not close to any of the scenarios by which the DL model was trained. Surprisingly, the DL model correctly detects and classifies the general trend of the  $EC_{\text{cat}}$  mechanism ( $\text{RoI}_4$ ), amid one  $fp_3$  ( $\text{RoI}_1$ ) and two  $fp_2$  ( $\text{RoI}_2$  and  $\text{RoI}_3$ ) cases with high  $\varphi$  propensities ( $> 75\%$ ) (Fig. 4K). It is interesting that both  $fp_2$  cases correctly detect redox events beyond the background and the second most likely mechanism is  $EC_{\text{cat}}$  for both (6.13% and 16.3%, respectively). Our results suggest that the EchemNet may still be used for voltammograms with fewer scan rates ( $n < 6$ ), yet prone to false-positive outputs. Practically, the issue of false-positives can be addressed in post-analysis by removing any detections whose  $\varphi$  propensity is larger than a threshold (say, 60% based on Fig. 4J and 4K). Our results hint that the EchemNet could be “stretched” a bit for the analysis of scenarios new to the model (more discussion in Supplementary Note 8), but a more systematic evaluation ought to be conducted in the future.

The reported EchemNet model was further deployed to analyze voltammograms of polished Pt disk electrode in 1 M  $\text{H}_2\text{SO}_4$  under  $\text{N}_2$  environments (Fig. 4L, see Supplementary Note 6). As a classic textbook example of electrochemically active materials,<sup>2</sup> within the solvent window four major features are expected: the cathodic proton-reduction reaction, the surface bound hydrogen underpotential deposition, the surface redox chemistry of oxide formation, the anodic water-oxidation reaction. The developed DL model correctly identified the surface redox of hydrogen underpotential deposition ( $\text{RoI}_2$ ,  $y_{\text{SR}} = 88.5\%$ ), as well as the anodic water oxidation reaction ( $\text{RoI}_3$ ,  $y_{\text{T}} = 89.7\%$ ). However, the DL model has mis-assigned the cathodic proton reduction as  $EC_{\text{cat}}$  ( $EC'$ ) mechanisms in  $\text{RoI}_1$  ( $fp_2$ ). The surface oxide redox was detected as  $\text{RoI}_5$ , but mechanistically designated primarily as double-layer capacitive charging ( $y_\varphi = 93.4\%$ ) with surface redox ( $y_{\text{SR}} = 5.32\%$ ) as the second most probable mechanism.

In Fig. 4L, the misassignment of  $\text{RoI}_1$  is possibly due to the feature of  $\text{H}_2$  re-oxidation in the voltammogram (highlighted

as \* in Fig. 4L) that was not part of the training dataset designed as  $T$  mechanism (See Supplementary Note 3). The mis-assignment of  $\text{RoI}_5$  is hypothesized to originate from the small and relatively broad feature of surface oxide on Pt, as the training data were established with a minimal ratio of 5 between the redox signal and the double-layer capacitive charging (See Supplementary Note 3 and Table S1). Our results suggest much room of improvements for the EchemNet's deployment on more complicated electrochemical systems. The mis-assignment in  $\text{RoI}_1$  highlights the importance of proper training set that includes all the possible variations in a certain mechanism; the unsatisfying assignment in  $\text{RoI}_5$  suggests that the DL model should be more sensitive (*i.e.* higher weights) towards small redox features when the signal intensity is comparable to the double-layer capacitive current.

## CONCLUSION

In this work, we demonstrated the feasibility of a DL model to detect and analyze redox features in cyclic voltammograms of multiple redox events. We developed a custom-designed Faster R-CNN architecture that tailors to the 1D data format in electrochemical characterizations. Furthermore, we evaluated the DL model's performance against simulated and some exemplary experimental voltammograms. Such an EchemNet model aligns well with the need for high-throughput data analysis in a general-purpose autonomous electrochemistry platform, which is expected to automatically analyze experimentally measured data on-the-fly with little if any *a priori* knowledge of the chemical system and transduce the available finite information from the analytical results into a decision-making process for the next robotic experiment execution. The EchemNet model's capability of detecting an arbitrary number of redox events is commensurate with a data analysis process that accommodates a wide range of redox events, expected or unexpected, with little if any *a priori* chemistry knowledge.

The inner working of our DL model resembles if not repeats the numerical simulation/fitting procedures classically applied in quantitative mechanistic analysis of voltammograms (Fig. S5). As commonly quipped as a fancy fitting program, a DL model conducts classification tasks by numerically fitting through neural networks of various architectures. Therefore, when a DL model is asked to analyze a new voltammogram, effectively the model numerically “fits” the voltammogram in a single-pass against all the PDEs defined by their corresponding mechanisms in a parallel manner, instead of the iterative manner in the classic approach (Fig. S5). Although numerical simulation/fitting remains needed in the DL-based analysis to extract quantitative thermodynamic/kinetic information, the probabilistic manner of DL analysis differs from the classic one that relies heavily on the manual selection of mechanism formalism and the resultant PDEs.

The DL model's probabilistic approach of mechanistic classification avoids deterministic mechanistic assignments, undesired when only finite information is available during the experimental exploration, and allows for a decision-making process based on the analyzed propensity distribution. As showcased in our recent experimental demonstration,<sup>20</sup> our EchemNet model will augment the productivity of human researchers (more discussion in Supplementary Note 9).

Additional research of the DL model is needed in order to achieve the aforementioned functionality in an autonomous electrochemistry platform (more discussion in Supplementary

Note 10). In particular, additional deployment of the DL model towards a large dataset of experimental voltammograms with diverse mechanisms is desired to further evaluate if not validate the model's utility in real-life applications. Noting the tremendous benefits of public datasets in the field of image recognition,<sup>31,32</sup> we call for the establishment of a public database of curated experimental voltammograms with a wide range of mechanisms. Such a public database will not only help benchmark future models' performance but also provide the training set for additional model refinement. A synergistic combination of simulated voltammograms that numerically exhaust all possible mechanistic variations and experimental ones that offer the taste of real-life scenarios is hypothesized to yield an artificial intelligence of electrochemical mechanistic deciphering that rivals if not surpass human intelligence.

## ■ ASSOCIATED CONTENT

### Data Availability Statement

The python codes used for model establishment can be found at the GitHub: <https://github.com/ZeroWeight/redox-detecting>. The COMSOL/python files for the generation simulated voltammograms, the training data, and the variants of established DL models can be found at this google drive folder: <https://drive.google.com/drive/folders/1glkKm4kJnhcDZdhh3IsAHLr08dICL3eV?usp=sharing>.

### SI Supporting Information

The Supporting Information is available free of charge at <https://pubs.acs.org/doi/10.1021/acselectrochem.4c00014>.

Protocols for numerical simulations of cyclic voltammograms; detailed definitions of individual electrochemical mechanisms; protocols for establishing the DL model; methods for the experimental electrochemical data; and supplementary figures related to the DL architecture (PDF)

## ■ AUTHOR INFORMATION

### Corresponding Authors

**Cyrille Costentin** – *Université Grenoble-Alpes, DCM, CNRS, 38000 Grenoble, France*; [orcid.org/0000-0002-7098-3132](https://orcid.org/0000-0002-7098-3132); Email: [cyrille.costentin@univ-grenoble-alpes.fr](mailto:cyrille.costentin@univ-grenoble-alpes.fr)

**Quanquan Gu** – *Department of Computer Science, University of California Los Angeles, Los Angeles, California 90095, United States*; Email: [qgu@cs.ucla.edu](mailto:qgu@cs.ucla.edu)

**Chong Liu** – *Department of Chemistry and Biochemistry and California NanoSystems Institute, University of California Los Angeles, Los Angeles, California 90095, United States*; [orcid.org/0000-0001-5546-3852](https://orcid.org/0000-0001-5546-3852); Email: [chongliu@chem.ucla.edu](mailto:chongliu@chem.ucla.edu)

### Authors

**Benjamin B. Hoar** – *Department of Chemistry and Biochemistry, University of California Los Angeles, Los Angeles, California 90095, United States*

**Weitong Zhang** – *Department of Computer Science, University of California Los Angeles, Los Angeles, California 90095, United States*

**Yuanzhou Chen** – *Department of Computer Science, University of California Los Angeles, Los Angeles, California 90095, United States*

**Jingwen Sun** – *Department of Chemistry and Biochemistry, University of California Los Angeles, Los Angeles, California 90095, United States*; [orcid.org/0000-0003-3657-7672](https://orcid.org/0000-0003-3657-7672)

**Hongyuan Sheng** – *Department of Chemistry and Biochemistry, University of California Los Angeles, Los Angeles, California 90095, United States*

**Yucheng Zhang** – *The Oden Institute for Computational Engineering and Sciences, The University of Texas at Austin, Austin, Texas 78712, United States*

**Yisi Chen** – *Department of Chemistry and Biochemistry, University of California Los Angeles, Los Angeles, California 90095, United States*

**Jenny Y. Yang** – *Department of Chemistry, University California Irvine, Irvine, California 92697, United States*; [orcid.org/0000-0002-9680-8260](https://orcid.org/0000-0002-9680-8260)

Complete contact information is available at:

<https://pubs.acs.org/10.1021/acselectrochem.4c00014>

### Author Contributions

<sup>†</sup>(B.B.H., W.Z., and Y.C.) These authors contributed equally. C.L. and Q.G. supervised the project. B.B.H., C.C., and C.L. developed the theoretical computational frameworks for the generation of simulated cyclic voltammograms. Y.Z. provided python scripts for SR mechanism data generation. W.Z., YZ.C., and Q.G. established the machine learning architecture. B.B.H. generated and sanitized the data necessary for model training/validation, and evaluated the established machine-learning model. J.S., H.S., and YS.C. conducted and analyzed experimental voltammograms with the developed model. B.B.H. wrote the initial manuscript draft, C.C. and J.Y.Y. provided critical philosophical insights, and C.L. finalized the manuscript. All of the authors discussed the results of the project and assisted with manuscript preparation.

### Notes

The authors declare the following competing financial interest(s): B.B.H., W.Z., Y.C., Q.G., and C.L. have filed a provisional patent for the work reported here.

## ■ ACKNOWLEDGMENTS

J.Y.Y., Q.G. and C.L. acknowledge the National Science Foundation (NSF) (CHE-2247426), W.Z. acknowledges the UCLA Dissertation Year Fellowship, C.C. acknowledges the partial support from Agence Nationale de la Recherche (Labex ARCANÉ, CBH-EUR-GS, ANR-17-EURE-0003). The authors thank Prof. Matthew Sigman and Dr. Avijit Hazra for constructive discussions. C.L. is grateful for the feedback from the attendees in the 2023 Telluride Workshop "Molecular Transformation through Proton-Coupled Electron Transfer for Energy Storage and Conversion". C.L. thanks the constructive interactions with "echem", a *Felis catus* at his residence that inspired the naming of EchemNet.

## ■ REFERENCES

- (1) Nicholson, R. S. Theory and Application of Cyclic Voltammetry for Measurement of Electrode Reaction Kinetics. *Anal. Chem.* **1965**, *37* (11), 1351–1355.
- (2) Bard, A. J.; Faulkner, L. R.; White, H. S. *Electrochemical Methods: Fundamentals and Applications*; John Wiley & Sons, Inc., 2022.
- (3) Savéant, J.-M.; Costentin, C. *Elements of Molecular and Biomolecular Electrochemistry: An Electrochemical Approach to Electron Transfer Chemistry*; John Wiley & Sons, Inc., 2019.
- (4) Compton, R. G.; Banks, C. E. *Understanding Voltammetry*; World Scientific Publishing Co Pte Ltd, 2018.
- (5) Eliaz, E. G. N. *Physical Electrochemistry: Fundamentals, Techniques, and Applications*; Wiley, 2019.

- (6) Elgrishi, N.; Rountree, K. J.; McCarthy, B. D.; Rountree, E. S.; Eisenhart, T. T.; Dempsey, J. L. A Practical Beginner's Guide to Cyclic Voltammetry. *J. Chem. Educ.* **2018**, *95* (2), 197–206.
- (7) Britz, D.; Strutwolf, J. *Digital Simulation in Electrochemistry*; Springer, 2016.
- (8) Sun, J.; Liu, C. What and how can machine learning help to decipher mechanisms in molecular electrochemistry? *Curr. Opin. Electrochem.* **2023**, *39*, 101306.
- (9) Gundry, L.; Guo, S. X.; Kennedy, G.; Keith, J.; Robinson, M.; Gavaghan, D.; Bond, A. M.; Zhang, J. Recent advances and future perspectives for automated parameterisation, Bayesian inference and machine learning in voltammetry. *Chem. Commun.* **2021**, *57* (15), 1855–1870.
- (10) Chen, H.; Kätelhön, E.; Compton, R. G. Machine learning in fundamental electrochemistry: Recent advances and future opportunities. *Curr. Opin. Electrochem.* **2023**, *38*, 101214.
- (11) Kennedy, G. F.; Zhang, J.; Bond, A. M. Automatically Identifying Electrode Reaction Mechanisms Using Deep Neural Networks. *Anal. Chem.* **2019**, *91* (19), 12220–12227.
- (12) Hoar, B. B.; Zhang, W.; Xu, S.; Deeba, R.; Costentin, C.; Gu, Q.; Liu, C. Electrochemical Mechanistic Analysis from Cyclic Voltammograms Based on Deep Learning. *ACS Meas. Sci. Au* **2022**, *2* (6), 595–604.
- (13) Gundry, L.; Kennedy, G.; Bond, A. M.; Zhang, J. Establishing zone regions in cyclic voltammetry using unsupervised machine learning. *J. Electroanal. Chem.* **2023**, *942*, 117551.
- (14) Chen, H.; Katelhon, E.; Compton, R. G. Predicting Voltammetry Using Physics-Informed Neural Networks. *J. Phys. Chem. Lett.* **2022**, *13* (2), 536–543.
- (15) Chen, H.; Batchelor-McAuley, C.; Kätelhön, E.; Elliott, J.; Compton, R. G. A Critical Evaluation of Using Physics-Informed Neural Networks for Simulating Voltammetry: Strengths, Weaknesses and Best Practices. *J. Electroanal. Chem.* **2022**, *925*, 116918.
- (16) Chen, H.; Katelhon, E.; Compton, R. G. Rotating Disk Electrodes beyond the Levich Approximation: Physics-Informed Neural Networks Reveal and Quantify Edge Effects. *Anal. Chem.* **2023**, *95* (34), 12826–12834.
- (17) Bishop, C. M. *Pattern Recognition and Machine Learning*; Springer, 2006.
- (18) Schachterle, S. D.; Perone, S. P. Classification of voltammetric data by computerized pattern recognition. *Anal. Chem.* **1981**, *53* (11), 1672–1678.
- (19) He, K.; Zhang, X.; Ren, S.; Sun, J. Deep Residual Learning for Image Recognition. *2016 IEEE Conference on Computer Vision and Pattern Recognition (CVPR)*; IEEE, 2016; pp 770–778.
- (20) Sheng, H.; Sun, J.; Rodríguez, O.; Hoar, B. B.; Zhang, W.; Xiang, D.; Tang, T.; Hazra, A.; Min, D. S.; Doyle, A. G.; et al. Autonomous closed-loop mechanistic investigation of molecular electrochemistry via automation. *Nature Commun.* **2024**, *15*, 2781.
- (21) Gerroll, H. R.; Kulesa, K.; Ault, C. A.; Baker, L. A. Legion: an instrument for high-throughput electrochemistry. *ACS Meas. Sci. Au* **2023**, *3*, 371–379.
- (22) Rein, J.; Annand, J. R.; Wismer, M. K.; Fu, J.; Siu, J. C.; Klapers, A.; Strotman, N. A.; Kalyani, D.; Lehnerr, D.; Lin, S. Unlocking the Potential of High-Throughput Experimentation for Electrochemistry with a Standardized Microscale Reactor. *ACS Cent. Sci.* **2021**, *7*, 1347–1355.
- (23) Oh, I.; Pence, M. A.; Lukhanin, N. G.; Rodríguez, O.; Schroeder, C. M.; Rodríguez-López, J. The Electrolab: An open-source, modular platform for automated characterization of redox-active electrolytes. *Device* **2023**, *1*, 100103.
- (24) Ren, S.; He, K.; Girshick, R.; Sun, J. Faster R-CNN: Towards Real-Time Object Detection with Region Proposal Networks. *Advances in Neural Information Processing Systems 28 (NIPS 2015)* **2017**, *39*, 1137.
- (25) Taha, A. A.; Hanbury, A. Metrics for evaluating 3D medical image segmentation: analysis, selection, and tool. *BMC Med. Imaging* **2015**, *15*, 29.
- (26) Gao, R.; Edwards, M. A.; Harris, J. M.; White, H. S. Shot noise sets the limit of quantification in electrochemical measurements. *Curr. Opin. Electrochem.* **2020**, *22*, 170–177.
- (27) Lin, T.-Y.; Dollár, P.; Girshick, R.; He, K.; Hariharan, B.; Belongie, S. Feature Pyramid Networks for Object Detection. *2017 IEEE Conference on Computer Vision and Pattern Recognition (CVPR)*; 2017; pp 2117–2125.
- (28) Costentin, C.; Passard, G.; Robert, M.; Savéant, J.-M. Concertedness in proton-coupled electron transfer cleavages of carbon–metal bonds illustrated by the reduction of an alkyl cobalt porphyrin. *Chem. Sci.* **2013**, *4* (2), 819–823.
- (29) Rafiee, M.; Miles, K. C.; Stahl, S. S. Electrocatalytic Alcohol Oxidation with TEMPO and Bicyclic Nitroxyl Derivatives: Driving Force Trumps Steric Effects. *J. Am. Chem. Soc.* **2015**, *137* (46), 14751–14757.
- (30) Nutting, J. E.; Rafiee, M.; Stahl, S. S. Tetramethylpiperidine N-Oxyl (TEMPO), Phthalimide N-Oxyl (PINO), and Related N-Oxyl Species: Electrochemical Properties and Their Use in Electrocatalytic Reactions. *Chem. Rev.* **2018**, *118* (9), 4834–4885.
- (31) Deng, J.; Dong, W.; Socher, R.; Li, L. J.; Kai, L.; Li, F.-F. ImageNet: A large-scale hierarchical image database. In *2009 IEEE Conference on Computer Vision and Pattern Recognition*, 20–25 June 2009, 2009; pp 248–255.
- (32) Lin, T.-Y.; Maire, M.; Belongie, S.; Hays, J.; Perona, P.; Ramanan, D.; Dollár, P.; Zitnick, C. L. Microsoft COCO: Common Objects in Context. In *Computer Vision—ECCV 2014*; Springer International Publishing; pp 740–755.